Journal of Energy Chemistry 80 (2023) 452–457

Contents lists available at ScienceDirect

Journal of Energy Chemistry

journal homepage: www.elsevier.com/locate/jechem

http://www.journals.elsevier.com/journal-of-energy-chemistry/

Morphological peculiarities of the lithium electrode from the perspective of the Marcus-Hush-Chidsey model

Behnam Ghalami Choobar [a,b], Hamid Hamed [a,b], Mohammadhosein Safari [a,b,c,*]

[a] Institute for Materials Research (IMO-imomec), UHasselt, Martelarenlaan 42, B-3500 Hasselt, Belgium
[b] Energyville, Thor Park 8320, B-3600 Genk, Belgium
[c] IMEC Division IMOMEC, BE-3590, Belgium

ARTICLE INFO

Article history:
Received 5 December 2022
Revised 23 January 2023
Accepted 25 January 2023
Available online 14 February 2023

Keywords:
Marcus-Hush-Chidsey kinetics
Surface orientation
Surface charge
Lithium electrode

ABSTRACT

This study employs the kinetics framework of Marcus-Hush-Chidsey (MHC) to investigate the charge transfer at the interface of lithium electrode and electrolyte in lithium(ion)-batteries. The charge-transfer rate constant is evaluated for different facets of lithium, namely (1 0 0), (1 1 0), (1 0 1), and (1 1 1) as a function of surface charge density with the aid of density functional theory (DFT) calculations. The results highlight and quantify the sensitivity of the rate of lithium plating and stripping to the surface orientation, surface charge density, and charge-transfer over-potential. An intrinsic kinetics competition among the different surface orientations is identified together with an asymmetry between the lithium plating and stripping and showcased to influence the deposit morphology and surface protrusions and indentations.

1. Introduction

The ever-increasing demand for batteries with higher energy densities propels the battery research community towards the realization of alternative solutions with superior energy and power characteristics. The lithium metal anode, thanks to its high theoretical capacity of 3860 mAh/g, is a favored anode for the next generation batteries, such as all-solid-state lithium, lithium-ion and lithium-sulfur batteries [1]. The lithium metal, however, is prone to surface instabilities in contact with the electrolyte as well as dendrite growth on account of its low surface energy [2] and high surface diffusion barrier [3] raising the safety concerns of the short-circuit and thermal runaway [1,4]. The physics-based modeling at the macroscopic [5–9] and molecular [2,10–12] scales have provided invaluable insights into the causes and effects of the failure mechanisms for the lithium electrode, facilitating the design of new materials [13–15] and mitigation strategies [10,16–18]. The investigations of the thermodynamics and kinetics origins of the surface instabilities during lithium plating form the major body of the current modeling literature [11,19] while a recent growing number of reports highlight and quantify the important role of the lithium stripping step in triggering the loss of contact via hole formation and intensifying the dendrite growth in the subsequent plating steps [20–23]. The transition from the pseudo-epitaxial to mossy and dendritic regimes of growth was explained in a thermodynamics context by identifying a critical potential threshold below which a negative surface tension would favor the increase of the surface area over bulk [2,4,10–12,24]. The earlier kinetic interpretations, on the other hand, explained the onset of plating instability to the transition from a reaction-limited (random deposition) to a transport-limited (Sand's time) regime [25]. The charge-discharge simulation of the lithium electrode based on the conventional macroscopic models suggests that the distinctive features of the lithium electrode under practical operating conditions cannot be solely attributed to the transport properties of the electrolyte, e.g., ion depletion at lithium/electrolyte interface (Fig. S1).

Despite its significance, the modeling of the charge transfer kinetics at the lithium/electrolyte interface has been less explored [26] and mostly treated by the Butler-Volmer (BV) model, which is in common use for lithium-ion batteries (LIBs) [27,28]. In contrast to the conventional insertion-based anodes of LIBs, lithium electrode deserves a more comprehensive kinetics modeling framework [27,29,30] to facilitate explaining its peculiar features such as voltage hysteresis (plating/stripping asymmetry) [11,31] and its morphological sensitivity to the surface charge density [32] and the composition of the electrolyte and additives [15,33,34], among others. Marcus-Hush-Chidsey (MHC) kinetic model is a

* Corresponding author.
E-mail address: momo.safari@uhasselt.be (M. Safari).

https://doi.org/10.1016/j.jechem.2023.01.059

powerful alternative framework [29,35] that has successfully been employed to describe the charge transfer reactions for various electrochemical systems [29,30,36,37]. MHC model considers the occupation of the electronic states in the electrode and energetics of the solvent reorganization prior to the electron transfer. Although these extra considerations, relative to a Butler-Volmer framework, complicate the application of the MHC, but in the present study, its added values are showcased for the analysis of the charge transfer kinetics at the interface between lithium and a typical solid polymer electrolyte. To do so, the density of states (DOS) is calculated and used together with the MHC model to quantify the reactivity of the lithium electrode and its sensitivity to the surface orientation and charge density.

2. Results and discussion

In line with the previous reports [2,11], our calculations (Table S2) suggest that the (1 1 0) orientation of lithium has the largest work function and the smallest surface energy, making it a thermodynamically favorable surface to be formed during the lithium deposition. The lower surface energy, however, renders the surface more vulnerable to the fluctuations and hence the formation of the whiskers and dendrites [32]. DFT calculations were performed to calculate the DOS of uncharged and charged lithium surfaces (0, 10, −10, −15, and −20 μC/cm^2). DOS profiles (Fig. 1) reflect the expected metallic behavior and the availability of the energy states at the Fermi level with the overlap of the conduction and valence bands [29,36]. Noteworthy is the significant sensitivity of the DOS to the orientation and charge density of the surface and the energy level (Fig. 1). The latter observation calls into question the legitimacy of assuming a flat DOS in the computation of the kinetics rate constants [36]. According to a simple jellium model, in the Li bulk the DOS is constant in the direction perpendicular to the surface, but the abrupt lattice termination near the surface results in a non-uniform DOS which is the origin of the well-known surface dipole or surface potential contribution (χ) to the work function (φ) [38].

$$\varphi = -\frac{\mu}{F} + \chi \tag{1}$$

where μ is the chemical potential of electron in Li metal and F is Faraday constant. The charge redistribution at the surface is a strong function of the crystallographic orientation and as such is a non-negligible factor in determining the work function. Although φ does not explicitly appears in the conventional electrochemical kinetics analysis, it is a more fundamental interpretation of the concept of over-potential and plays an important role in the electrode kinetics [39].

Although the uncharged (1 1 0) orientation has the most energy states at the Fermi level (Fig. 1a), the (1 0 0) orientation offers more electronic states for the circumstances with the positive (Fig. 1b) and negative deviations (Fig. 1c and d) from the potential-of-zero-charge (PZC).

Considering that the redox potential of Li^+/Li is lower relative to the PZC [32], under the practical operational conditions, the lithium electrode is negatively charged (Table S3). This situation suggests a kinetic preference for the participation of (1 0 0) and (1 1 1) orientations, in view of the available electronic states at the electrode, compared to the (1 1 0) and (1 0 1) orientations (Fig. 1d, Table S2). The computed DOS profiles once integrated into the MHC model (Eqs. (1) and (2), SI) provide the kinetics rate constants of lithium plating and stripping at different surface orientations and charge densities (Fig. 2). The results correspond to the lithium in contact with a typical polymer solid electrolyte with a reorganization energy of 0.18 eV [40] and are illustrated for a wide

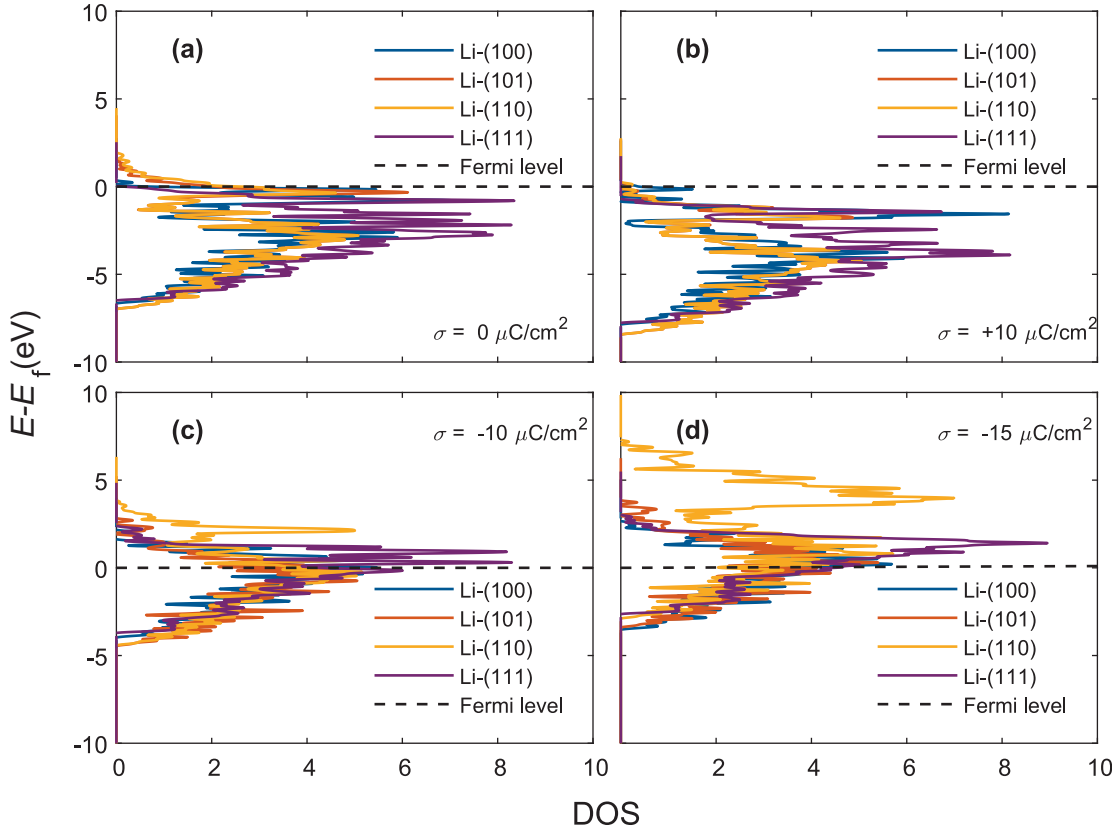

Fig. 1. DOS of (*hkl*) surface orientations of lithium computed at different surface charge densities of (a) 0 μC/cm^2, (b) 10 μC/cm^2, (c) −10 μC/cm^2, (d) −15 μC/cm^2.

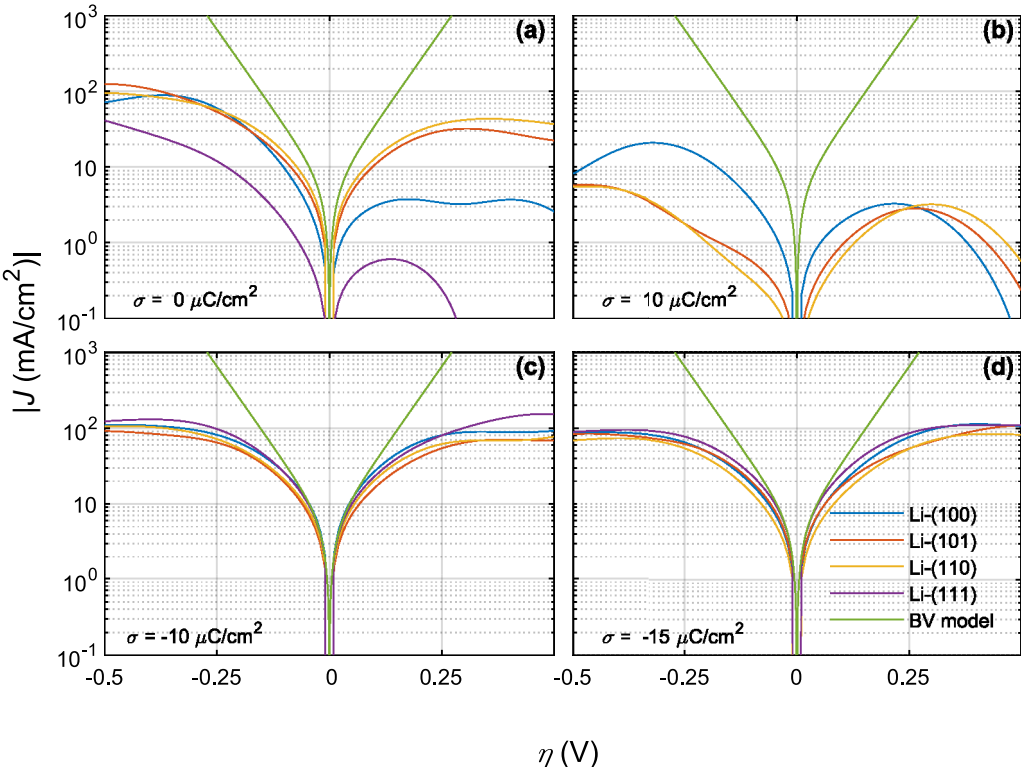

Fig. 2. Predicted rate constant for (*hkl*) different surface orientations of the lithium with different surface charge densities of (a) 0 μC/cm^2, (b) 10 μC/cm^2, (c) −10 μC/cm^2, (d) −15 μC/cm^2.

overpotential range of $|\eta| < 0.5$. This range, although rather high for practical applications, was selected to cover the possible local overshoots of voltage at a Li electrode on account of the non-uniform morphology and distribution of electrical states at the electrode/electrolyte interface. It is, however, noteworthy that the results should be taken as semiquantitative on account of the errors and model limitations common to the simulations at the molecular scales [41–45]. The rate constants vary among different orientations and demonstrate an asymmetry between plating and stripping. These features are more pronounced for the surfaces with a non-negative charge density value (Fig. 2a and b). Notwithstanding the orientation and charge, the $J-\eta$ plots exhibit a visible deviation from the BV behavior (green lines, Fig. 2) starting at overpotential values as small as 50 mV. The more practical relevance of the kinetics' sensitivity to the surface charge density and orientation is better understood in the context of the recent experimental and theoretical findings where the spatial distribution of the potential in the solid and electrolyte phases are shown to lead to a non-uniform distribution of the local ionic current density and over-potential at the electrode/electrolyte interface. For instance, in a recent experimental report by us, a significant spatial variation of the lithium thickness and roughness over the course of cycling was explained by the non-uniform distribution of the ionic current and potential in-plane of the lithium electrode surface [46]. From a more microscopic point of view, such a distribution of the potential drop at the electrode/electrolyte interface is a manifestation of a non-uniform distribution of the local charge density over the surface of the Li electrode. In this regard, Santos and Schmickler highlighted the crucial role of the local surface charge density on the formation dynamics of the dendrites [32]. Therefore, the kinetics simulations in Fig. 2 indirectly emulate the sensitivity of the local kinetics behavior of a Li electrode featuring a surface (2D) over which the electrical state of the interface is non-uniformly distributed either induced by the uneven morphological details or the non-uniform distribution of adatoms at the interface, among others. In this regard, one might look at the different J-η subplots of Fig. 2 as different kinetics' signature of a Li electrode once at different orientations and carrying different surface charge densities. In a more practical sense, if f describes the correlation between J and η, i.e. $J = f(\eta,(hlk),\sigma)$, then the multiplicity of trends observed in Fig. 2 implies that the local charge-transfer resistance (R_{ct} from a Nyquist impedance plot) of a Li electrode will be dependent on both surface orientation and local charge density, i.e. $R_{ct} = \left[\frac{\partial f}{\partial V}|_{\sigma,(hlk)}\right]^{-1}$ [47].

In this regard, the higher surface charge density at the surface indentations and protrusions will imply a locally higher overpotential supported by the calculated potentials as a function of surface charge density (Table S3). The results suggest an average variation of 140 mV for every 1 μC/cm^2 change in the surface charge density with (1 1 0) and (1 0 0) surfaces identified as the most and the least sensitive orientations to the local variations of charge density, respectively (Table S3). The wide distribution of the local stripping and plating kinetics as a function of the surface charge density and orientation is better illustrated in Fig. 3 for different ranges of surface overpotential (η). A lumped plating (stripping) power index (γ) was defined as the area under the $J-\eta$ plots (Fig. 2), i.e. $\gamma = \int J d\eta$, in order to facilitate the comparison of the plating and stripping kinetics among various orientations at different zones of η. Noteworthy is a rather broad distribution of the participation of different orientations in the plating and stripping process (Fig. 3). On average, a more uniform participation among the different orientations is observed at higher over-potentials (Figs. 3 and 4). The presence of negative charge density on the Li surface demonstrates a similar equalizing effect in kinetics activity of the different orientations (Figs. 3 and 4). Particularly, the (1 1 1) orientation is identified as the most kinetically active

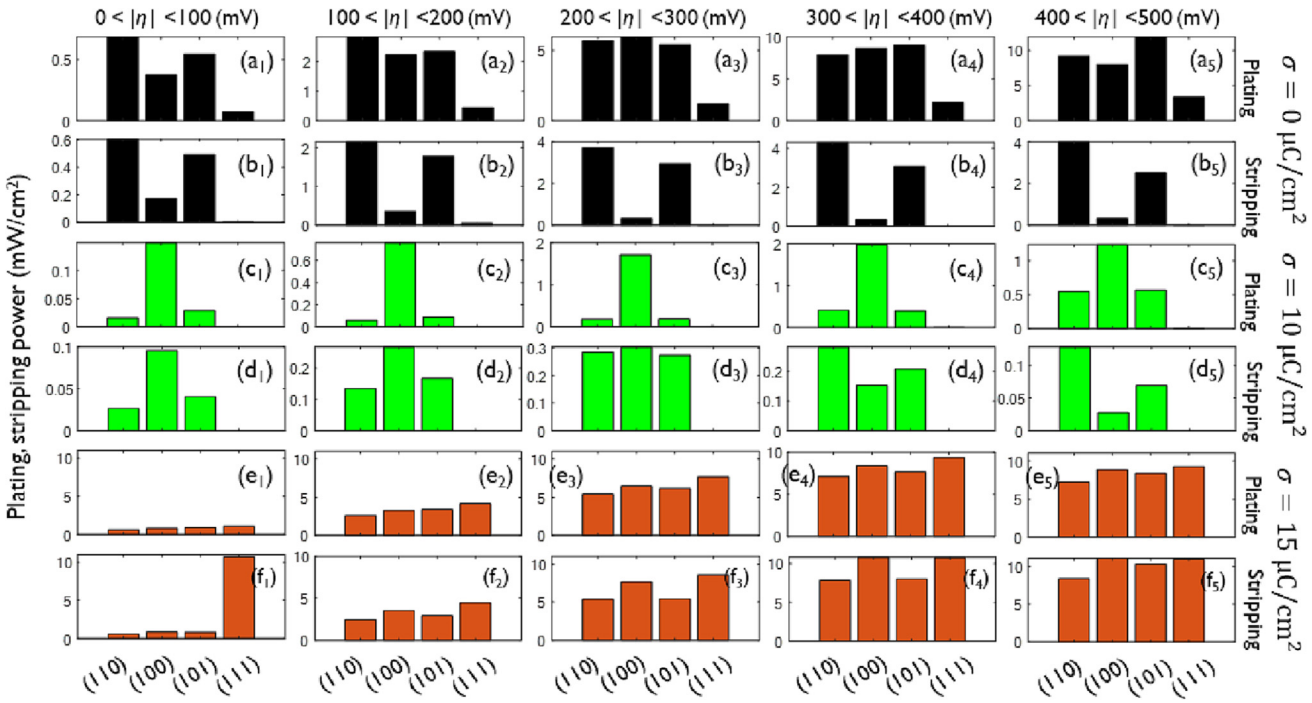

Fig. 3. The distribution of the plating/stripping power (γ) among (1 1 0), (1 0 0), (1 0 1), and (1 1 1) Li surface orientations at various charge densities (a_1–b_5) σ = 0 μC/cm^2, (c_1–d_5) σ = 10 μC/cm^2, (e_1–f_5) σ = −15 μC/cm^2, in different zones of charge-transfer over-potential.

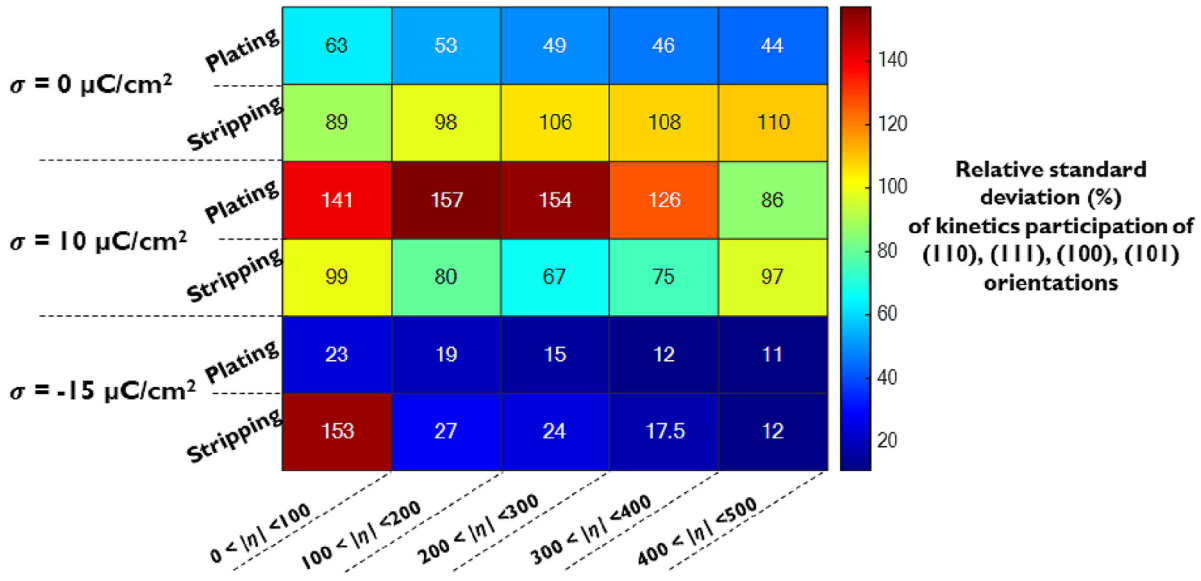

Fig. 4. Relative standard deviation of the plating/stripping power with respect to the (1 1 0), (1 0 0), (1 0 1) and (1 1 1) orientations in different zones of over-potential and at 3 different surface charge density conditions, i.e. 0, 10, and −15 μC/cm^2. The data are generated based on the plating/stripping power of the individual orientations (Fig. 3).

orientation at σ = −15 μC/cm^2 while being hardly active at non-negatively charged surfaces (Fig. 3).

One might use the relative standard deviation of the γ (RSD (γ)) to explain the sensitivity of the texture and morphology of the lithium electrode to the charge-transfer kinetics' parameters, including the surface over-potential and surface charge density (Fig. 4). RSD (γ) might be interpreted as a gauge to measure the competition degree of the charge-transfer kinetics among different surface orientations during lithium plating and stripping. A larger RSD (γ) represents a more preferential growth or dissolution for a particular orientation resulting in a more anisotropic and textured particle morphology. Such a kinetically favored orientation if positioned perpendicular to the electrode surface is then more vulnerable to the dendritic growth. A less faceted morphology, on the contrary, might be indexed to lower values of RSD (γ). In this regard, our results suggest that irrespective of the surface charge density, the lower charge-transfer over-potential (η) promotes the preferential plating and growth of lithium whereas this regime of growth is disfavored at higher η (Fig. 4). The kinetics competition among different surface orientations follows a more complicated pattern during lithium stripping. At σ = −15 μC/cm^2, lowering the η is in favor of preferential stripping. The opposite

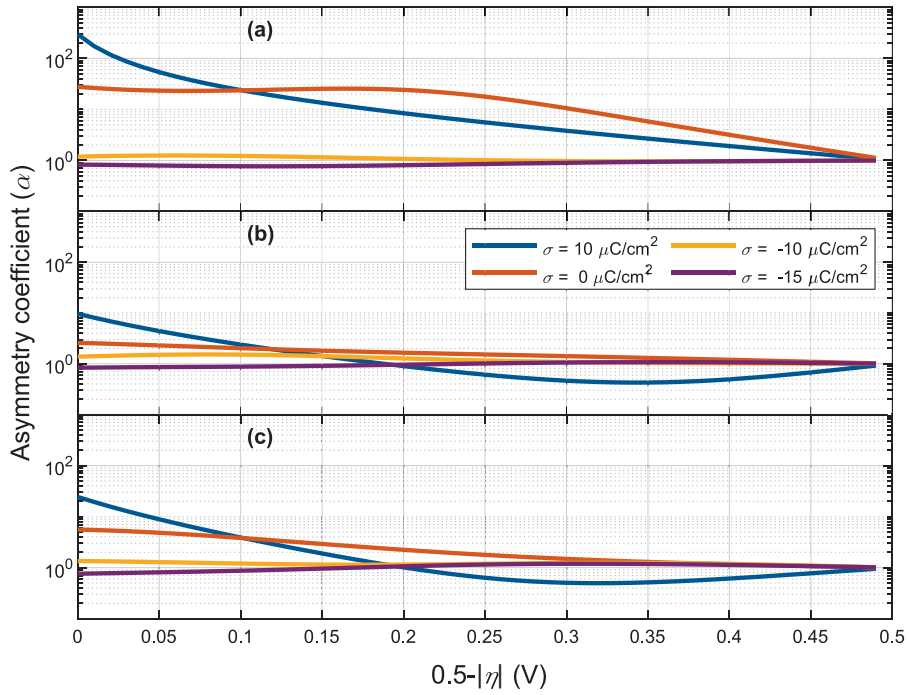

Fig. 5. The asymmetry between the lithium plating and stripping current with different surface charge densities of σ = 0, 10, −10, and −15 μC/cm^2 for the surface orientations of (a) (1 0 0), (b) (1 1 0), and (c) (1 0 1).

trend is observed at PZC, where the preferential stripping is promoted at higher η. At σ = 10 μC/cm^2, increasing the kinetics over-potential in the ranges of 0 < η < 300 mV and 300 < η < 500 mV hinders and enhances, respectively, the preferential stripping of lithium (Fig. 4).

The roughening of the lithium surface over continuous plating/stripping cycles is an important aging aspect of the lithium metal electrodes leading to the loss of contact and formation of dead lithium [23,48,49]. A charge-transfer-induced roughness is conceivable on account of the observed asymmetry between the plating (J_p) and stripping (J_s) current at a given over-potential (Fig. 5). The asymmetry coefficient defined as $\alpha = J_p/J_s$ deviates from unity except at very low over-potential values (η < 250 mV). The asymmetric behavior is particularly dominant for the non-negatively charged surfaces at higher over-potential with $\alpha \gg 1$. At higher η, however, the negatively charged surfaces exhibit 0.4 < α < 0.9. Noteworthy is the different deviation behavior of the α from unity among surface orientations which suggests a relative preferential accumulation or recess of the particular orientations over the cycle life of a lithium electrode. For instance, the variation trends of α (Fig. 5) suggest that the cycling at a high overpotential for a non-negatively charged surface tends to enrich the surface protrusions with the (1 0 0) orientation. Moreover, the (1 1 1) surface displays an extreme asymmetry ($\alpha \gg 1$) at PZC and for positively charged surfaces (Fig. 3a1–b5) over the entire range of over-potential contributing to the surface protrusions while sharing the same trends for negatively charged surfaces with other orientations. The negatively charged surfaces induce less severe asymmetry effects although both surface indentations and protrusions are equally present at higher over-potentials (Fig. 5).

Our results suggest that cycling a Li electrode under a kinetics-controlled regime at lower and higher overpotentials has a smoothing and freezing effect for the surface irregularities, respectively. This means that a Li anode would be more durable if cycled at lower overpotentials in contact with an ideal electrolyte where the concentration overpotentials are negligible. Moreover, although the Li surface with more negative charge densities is known to be more vulnerable to the dendrite growth from a thermodynamics point of view, the findings of this work suggest that from a charge-transfer kinetics standpoint a Li surface with a more negative surface charge density on average is more protected from the morphological non-uniformities on a longer-term cycling. In this regard, more attention should be devoted to the lithium stripping in devising the protection strategies for lithium electrode. One possible trajectory might be the use of electrolyte additives such as organic cations to fine-tune the electric double layer [50]. These findings remain qualitative and to be confirmed with the future experimental studies but they point out to the need for more sophisticated theoretical and experimental kinetics investigations to better understand and optimize the Li/electrolyte interface for Li-metal-based batteries.

3. Conclusions

This research employed the DFT calculations and Marcus-Hush-Chidsey model to shed light on the peculiar performance features of the lithium electrode in lithium-ion and lithium metal batteries in the context of the charge-transfer reaction at the lithium-electrolyte interface. The DFT calculations were performed to obtain the electronic density of states for different orientations of lithium with neutral and charged surfaces. The sensitivity of the rate constants and the plating/stripping asymmetry to the surface orientation and charge density was demonstrated to be significant. Two kinetic parameters were introduced to discuss the morphology and roughness features of the lithium electrode originating from its charge transfer behavior. The first parameter reflects the degree of kinetics competition between the different orientations and found responsible for determining the uniform or preferential regimes of growth and stripping of the lithium particles. The second parameter indexes the level of asymmetry between the plating and stripping current, which impacts the accumulation of the protrusions or indentations at the lithium surface over repeated

cycling. The results demonstrate the power of the MHC framework to bridge between the atomistic and molecular properties of the Li/electrolyte interface and the macroscopic features of the lithium electrode during deposition and stripping. This paves the road for a physics-based multi-scale simulation of the morphological evolution of a lithium electrode in lithium(ion) batteries and its sensitivity to the properties of the interface and operational conditions. In this respect, the following modeling works can target the coupling of the MHC with a macroscopic 2D Newman battery model to simulate the uneven deposition and stripping of the Li electrode under practical conditions. The simulations from such a model once matched with the experimental time-series of the voltage and current at different operating conditions and electrolyte compositions can provide invaluable insights to facilitate the optimization of the Li/electrolyte interface for lithium batteries.

Experimental section

Experimental details can be found in the Supporting Information.

Declaration of competing interest

The authors declare that they have no known competing financial interests or personal relationships that could have appeared to influence the work reported in this paper.

Acknowledgments

This work was supported by the European Union's Horizon 2020 Research and Innovation Program for the Solidify Project (875557).

Appendix A. Supplementary material

Supplementary material to this article can be found online at https://doi.org/10.1016/j.jechem.2023.01.059.

References

[1] T. Krauskopf, F.H. Richter, W.G. Zeier, J. Janek, Chem. Rev. 120 (2020) 7745–7794.
[2] K.S. Nagy, S. Kazemiabnavi, K. Thornton, D.J. Siegel, ACS Appl. Mater. Interfaces 11 (2019) 7954–7964.
[3] M. Jäckle, A. Groß, J. Chem. Phys. 141 (2014).
[4] X. Gao, Y.-N. Zhou, D. Han, J. Zhou, D. Zhou, W. Tang, J.B. Goodenough, Joule 4 (2020) 1864–1879.
[5] G. Bucci, J. Christensen, J. Power Sources 441 (2019).
[6] A. Mistry, P.P. Mukherjee, J. Electrochem. Soc. 167 (2020).
[7] P. Barai, K. Higa, V. Srinivasan, J. Electrochem. Soc. 165 (2018) A2654–A2666.
[8] C. Monroe, J. Newman, J. Electrochem. Soc. 152 (2005) A396.
[9] Z.-T. Sun, S.-H. Bo, J. Mater. Res. (2022), https://doi.org/10.1557/s43578-022-00558-6.
[10] B. Ghalami Choobar, H. Modarress, R. Halladj, S. Amjad-Iranagh, Comput. Mater. Sci. 192 (2021).
[11] A. Hagopian, M.-L. Doublet, J.-S. Filhol, Energy Environ. Sci. 13 (2020) 5186–5197.
[12] A. Hagopian, M.-L. Doublet, J.-S. Filhol, T. Binninger, J. Chem. Theory Comput. 18 (2022) 1883–1893.
[13] L. Zhang, S. Chen, W. Wang, H. Yu, H. Xie, H. Wang, S. Yang, C. Zhang, X. Liu, J. Energy Chem. 75 (2022) 408–421.
[14] D. Rakov, M. Hasanpoor, A. Baskin, J.W. Lawson, F. Chen, P.V. Cherepanov, A.N. Simonov, P.C. Howlett, M. Forsyth, Chem. Mater. 34 (2022) 165–177.
[15] S. Angarita-Gomez, P.B. Balbuena, Phys. Chem. Chem. Phys. 22 (2020) 21369–21382.
[16] Ozhabes Y., Gunceler D., Arias T.A., (2015) arXiv: 1504.05799
[17] A. Aryanfar, D. Brooks, B.V. Merinov, W.A. Goddard, A.J. Colussi, M.R. Hoffmann, J. Phys. Chem. Lett. 5 (2014) 1721–1726.
[18] A.V. Sergeev, A.A. Rulev, Y.O. Kondratyeva, L.V. Yashina, Acta Mater. 233 (2022).
[19] L. Blume, U. Sauter, T. Jacob, Electrochim. Acta 318 (2019) 551–559.
[20] M. Yang, Y. Mo, Angew. Chem. 133 (2021) 21664–21671.
[21] G. Yoon, S. Moon, G. Ceder, K. Kang, Chem. Mater. 30 (2018) 6769–6776.
[22] D. Tewari, P.P. Mukherjee, J. Mater. Chem. A 7 (2019) 4668–4688.
[23] X.-R. Chen, C. Yan, J.-F. Ding, H.-J. Peng, Q. Zhang, J. Energy Chem. 62 (2021) 289–294.
[24] D.R. Ely, R.E. García, J. Electrochem. Soc. 160 (2013) A662–A668.
[25] P. Bai, J. Li, F.R. Brushett, M.Z. Bazant, Energy Environ. Sci. 9 (2016) 3221–3229.
[26] C. Yan, R. Xu, Y. Xiao, J. Ding, L. Xu, B. Li, J. Huang, Adv. Funct. Mater. 30 (2020) 1909887.
[27] A. Latz, J. Zausch, Electrochim. Acta 110 (2013) 358–362.
[28] J.S. Newman, N.P. Balsara, Electrochemical Systems, 4th Ed., Wiley, Hoboken, NJ, 2019.
[29] P. Bai, M.Z. Bazant, Nat. Commun. 5 (2014) 3585.
[30] D.T. Boyle, X. Kong, A. Pei, P.E. Rudnicki, F. Shi, W. Huang, Z. Bao, J. Qin, Y. Cui, ACS Energy Lett. 5 (2020) 701–709.
[31] D. Koo, B. Kwon, J. Lee, K.T. Lee, Chem. Commun. 55 (2019) 9637–9640.
[32] E. Santos, W. Schmickler, Angew. Chem. Int. Ed. 60 (2021) 5876–5881.
[33] F. Shi, A. Pei, A. Vailionis, J. Xie, B. Liu, J. Zhao, Y. Gong, Y. Cui, Proc. Natl. Acad. Sci. 114 (2017) 12138–12143.
[34] F. Ding, W. Xu, G.L. Graff, J. Zhang, M.L. Sushko, X. Chen, Y. Shao, M.H. Engelhard, Z. Nie, J. Xiao, X. Liu, P.V. Sushko, J. Liu, J.-G. Zhang, J. Am. Chem. Soc. 135 (2013) 4450–4456.
[35] M.Z. Bazant, Acc. Chem. Res. 46 (2013) 1144–1160.
[36] R. Kurchin, V. Viswanathan, J. Chem. Phys. 153 (2020).
[37] S. Sripad, D. Korff, S.C. DeCaluwe, V. Viswanathan, J. Chem. Phys. 153 (2020).
[38] A. Kahn, Mater. Horiz. 3 (2016) 7–10.
[39] S. Trasatti, J. Electroanal. Chem. Interfacial Electrochem. 39 (1972) 163–184.
[40] M. Nookala, B. Kumar, S. Rodrigues, J. Power Sources 111 (2002) 165–172.
[41] B. Ghalami Choobar, H. Modarress, R. Halladj, S. Amjad-Iranagh, J. Phys. Chem. C 123 (2019) 21913–21930.
[42] S. Yang, X. Gao, Y. Li, W. Xie, B. Guo, L. Zhang, X. Liu, J. Power Sources 494 (2021).
[43] G. Varghese, V.B.K. P, T.V. Joseph, P. Chippar, Int. J. Hydrog. Energy 47 (2022) 33014–33026.
[44] K. Yassin, I.G. Rasin, S. Brandon, D.R. Dekel, J. Power Sources 524 (2022).
[45] C. Cai, D. Hensley, G.M. Koenig, J. Energy Storage 54 (2022).
[46] S. Yari Marlies, K. Van Bael, A. Hardy, M. Safari, Batter. Supercaps. 5 (2022) e202200217.
[47] M.E. Orazem, B. Tribollet, Electrochemical Impedance Spectroscopy, Wiley, Hoboken, N.J., 2008.
[48] S. Zhang, G. Yang, Z. Liu, S. Weng, X. Li, X. Wang, Y. Gao, Z. Wang, L. Chen, ACS Energy Lett. 6 (2021) 4118–4126.
[49] H.-K. Tian, Y. Qi, J. Electrochem. Soc. 164 (2017) E3512–E3521.
[50] Y.A. Budkov, A.V. Sergeev, S.V. Zavarzin, A.L. Kolesnikov, J. Phys. Chem. C 124 (2020) 16308–16314.